Supplemental Figures

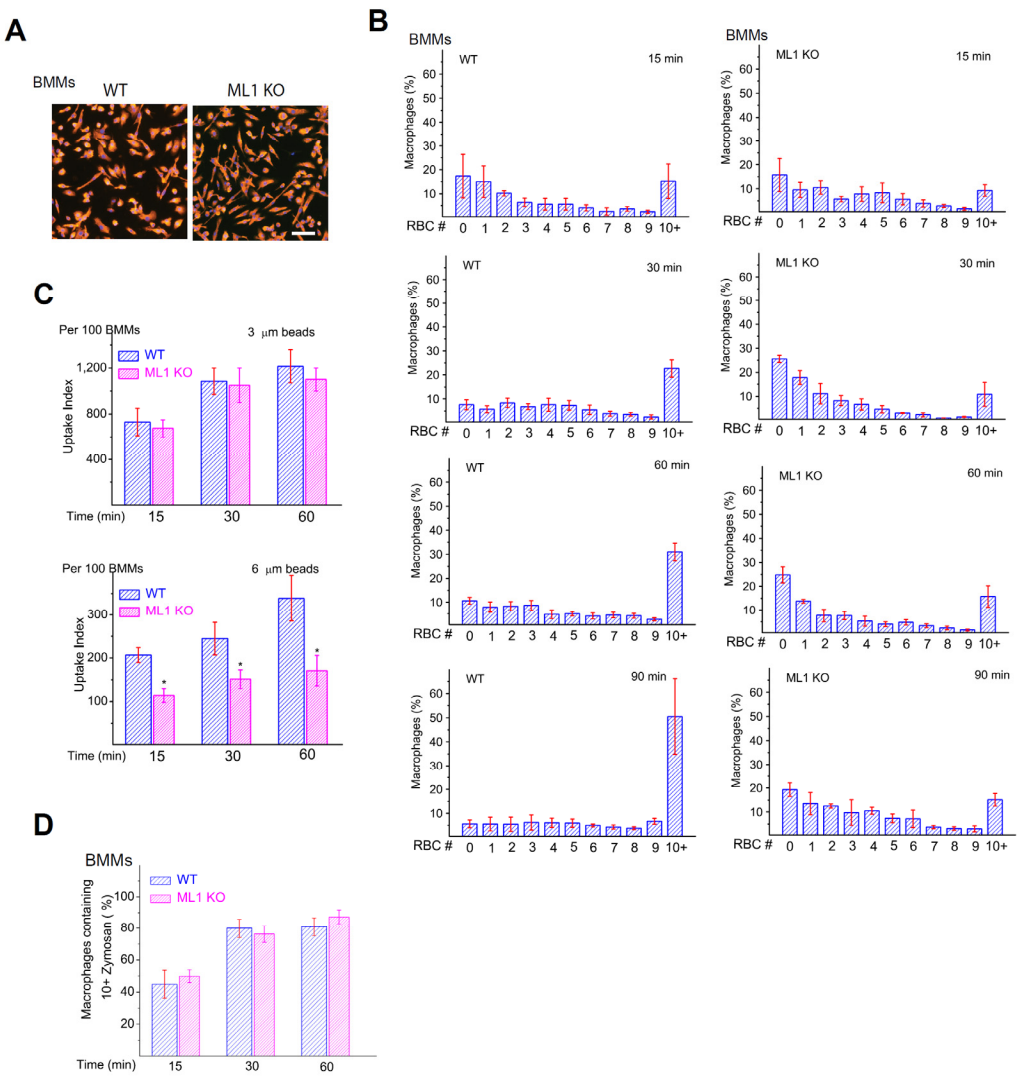

Suppl. Fig. S1. Uptake of large particles is reduced in ML1-null macrophages-- Related to Figure 1.

(A) Mature monocytes isolated from WT and ML1 KO mouse bone marrow had similar morphological characteristics as revealed by CD11b (mature macrophage-specific surface receptor) staining. Scale bar = 30 μm. Isolated monocytes were cultured in DMEM/F12 and recombinant colony stimulating factor for 5-7 days, and then fixed and stained with anti-CD11b antibody. **(B)** ML1 KO BMMs were defective in large particle uptake. Histograms represent the distribution (in percentage) of WT and ML1 KO BMMs containing different numbers of ingested RBCs (x-axis) for each time point. **(C)** ML1 KO BMMs had a lower uptake index for large, but not small beads compared with WT BMMs. Uptake index was calculated based on the total number of particles ingested for 100 BMMs. **(D)** Zymosan particle uptake was normal in ML1 KO BMMs. BMMs were exposed to Zymosan particles at 1:50 ratio for time periods indicated. For all panels, unless otherwise indicated, the data represent the mean ± the standard error of the mean (SEM) from at least three independent experiments.

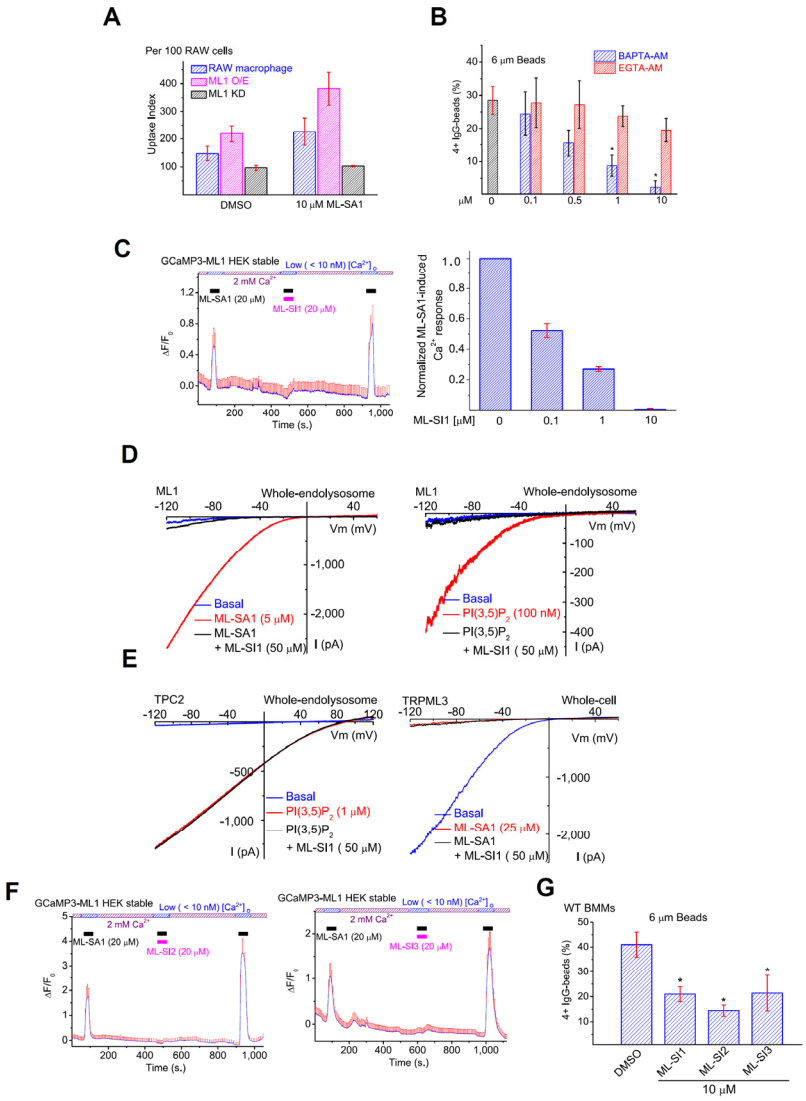

Suppl. Fig. S2. Phagocytosis of large particles in macrophages is inhibited by ML1 antagonists--Related to Figure 2.

(A) Particle uptake index in RAW 264.7, ML1 O/E, and ML1 KD RAW macrophages. **(B)** Dose-dependent inhibition of bead (6 μm) uptake in WT BMMs by BAPTA-AM, but not EGTA-AM at 30 min upon particle binding. **(C)** ML-SI1 (20 μM) inhibited ML-SA1-induced lysosomal Ca^{2+} increase in HEK293 cells stably expressing GCaMP3-ML1 (left panel). ML-SA1 induced rapid increases in GCaMP3 fluorescence (measured as change of GCaMP3 fluorescence ΔF over basal fluorescence F_0; ΔF/F0) under low (<10 nM) external Ca^{2+} in GCaMP3-ML1 stable cell lines. Co-application of ML-SI1 abolished the ML-SA1-induced lysosomal Ca^{2+} release. Right panel shows the dose-dependent inhibition of Ca^{2+} increase by ML1-SI1 in the micromolar range. **(D)** ML-SI1 inhibited ML-SA1 or $PI(3,5)P_2$-activated whole-endolysosome I_{ML1}. **(E)** Insensitivity of whole-endolysosome I_{TPC2} and sensitivity of whole-cell I_{TRPML3} to ML-SI1. I_{TPC2} and I_{TRPML3} were activated by $PI(3,5)P_2$ and ML-SA1, respectively. **(F)** ML-SI2 and ML-SI3 (20 μM each) inhibited ML-SA1-induced lysosomal Ca^{2+} increase in HEK293 cells stably expressing GCaMP3-ML1. **(G)** ML-SI1, ML-SI2, and ML-SI3 (10 μM each) inhibited the uptake of large IgG-beads (6 μm) in WT BMMs. For all panels, unless otherwise indicated, the data represent the mean ± the standard error of the mean (SEM) from at least three independent experiments.

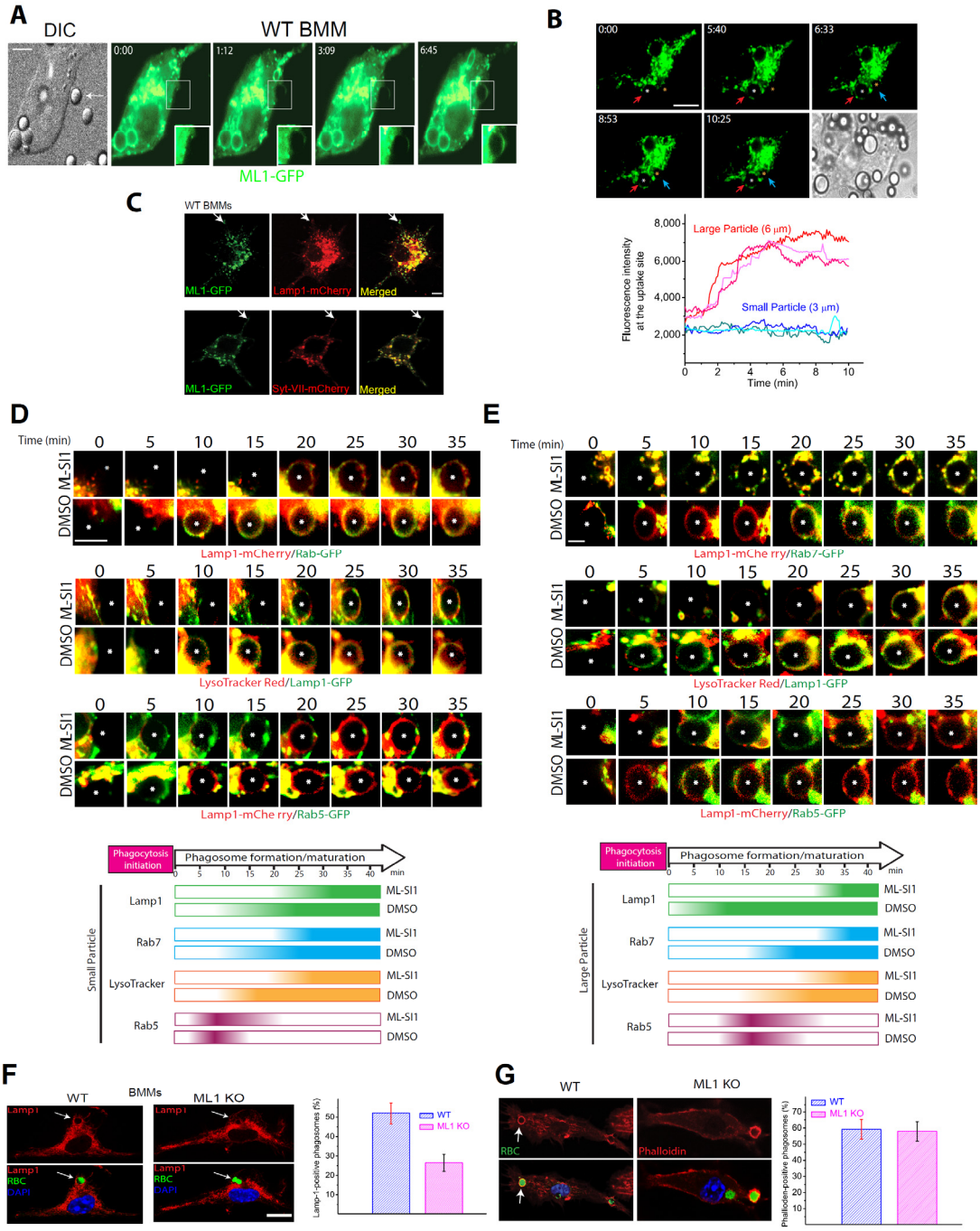

Suppl. Fig. S3. Rapid particle-size-dependent recruitment of lysosomal membrane proteins to the pseudopods of phagocytosing BMMs-- Related to Figure 3.

(A) Rapid recruitment of ML1-GFP to the sites of particle ingestion and to expanding membrane extensions. Selected frames from time-lapse confocal microscopy of a ML1-GFP transfected RAW 264.7 macrophage that was exposed to IgG-RBCs. Approximately one min after the attachment of RBCs to the cell surface, ML1-GFP was recruited to the membrane extension surrounding the particle

(Frame 1 min 12 sec; Video 2). Scale bar = 10 μm. **(B).** Particle-size-dependent recruitment of ML1-GFP to the uptake site. Time-lapse imaging of a ML1-GFP-transfected RAW 264.7 macrophage that was exposed to both large (6 μm) and small (3 μm) IgG-coated beads simultaneously. Approximately 5 min after the attachment of large beads to the cell surface (phagocytosis initiation), ML1-GFP was present at the membrane extensions surrounding a newly formed phagosome (red arrow, frame 5 min 40 sec). In contrast, for small beads, no significant ML1-GFP accumulation was seen surrounding the forming phagosome (blue arrow, frame 6 min 33 sec). The center of the particle is indicated with an *. Right panel showed the time-dependent changes of ML1-GFP fluorescence at the site of phagosome formation upon particle binding. N=3 for both large and small particles. Scale bar = 10 μm. **(C)** In RAW 264.7 cells doubly-transfected with ML1-GFP and Lamp1-mCherry, both ML1 and Lamp1 were co-localized at the tip of the pseudopods (arrows). **(D)** The effect of ML-SI1 on recruitment kinetics of different endolysosomal markers to the small particle-containing phagosomes. RAW macrophage cells were electroporated or labeled with various endosomal and lysosomal markers. Cells were pre-incubated with 20 μM ML-SI1 for 30 min, and then exposed to small (3 μm) IgG-coated beads in the continued presence of ML-SI1. Upon particle binding, the recruitment of molecular markers to phagosomes was monitored using live-cell imaging over the course of 40 min. The center of the particle is indicated with an *. Scale bars = 5 μm. Low panel summarizes the recruitment kinetics of various markers. **(E)** The effect of ML-SI1 on recruitment kinetics of different endolysosomal markers to the large particle-containing phagosomes. Compared with DMSO control, ML-SI1 prevented the early localization of Lamp1 to the forming early phagosomes, delayed the appearance of Rab7-GFP and LysoTracker in the late phagosomes, but without significantly affecting the recruitment of Rab5-GFP. The center of the particle is indicated with an *. Low panel summarizes the recruitment kinetics of various markers. Scale bars = 5 μm. (**F**) Early recruitment of Lamp1 to nascent phagosomes was defective in ML1 KO BMMs. BMMs were exposed to IgG-RBCs for 5 min, fixed, and stained with an anti-Lamp1 antibody (ID4B). Left panels: images represent the morphological criteria used to determine phagosome formation. Scale bar = 10 μm. Right panel: percentage of newly-formed phagosomes (5 min after particle binding) in WT and ML1 KO BMMs that were Lamp1-positive. Scale bar = 10 μm. **(G).** Actin polymerization of newly formed phagosomes, shown with phalloidin staining, was comparable in WT and ML1 KO BMMs. WT and ML1 KO BMMs were exposed to IgG-RBCs for 5 min, fixed, and labeled with phalloidin- Alexa-Fluor633 for 30 min. Left panel images represent the morphological criteria that were used to determine phagosome formation. The arrows point to RBC-containing phagosomes surrounded by phalloidin-stained polymerized actin. Right panel showed that about 60% of newly-formed phagosomes (5 min after particle binding) were Phalloidin positive in both WT and ML1 KO BMMs. For all panels, unless otherwise indicated, the data represent the mean ± the standard error of the mean (SEM) from at least three independent experiments.

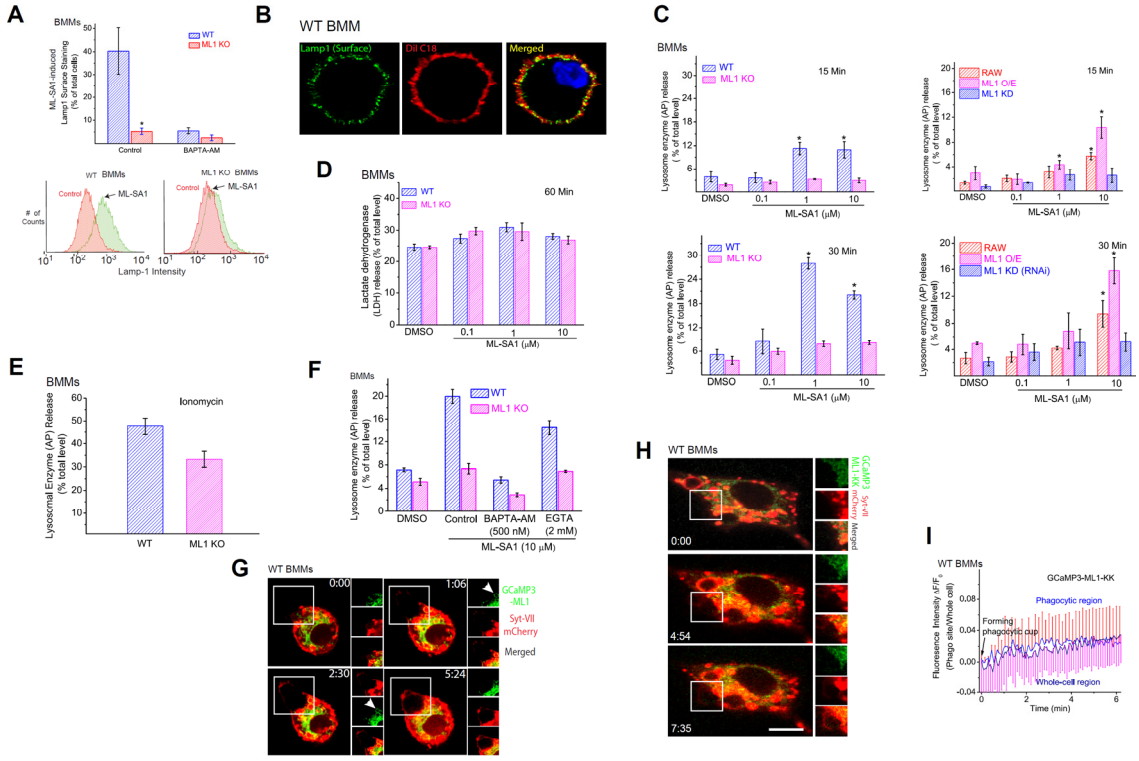

Suppl. Fig. S5. Lysosomal Ca^{2+} release and lysosomal exocytosis in the phagocytic sites upon particle binding--- Related to Figure 5.

(**A**) Flow cytometric analysis of ML-SA1-induced Lamp1 surface expression in WT and ML1 KO BMMs. Pre-treatment with BAPTA-AM (1 μM for 30 min) completely abolished Lamp1 surface staining in WT BMMs. Lower panels: histograms showing the flow cytometric analysis of Lamp1 surface staining. **(B)** Lamp1 surface staining was co-localized with the plasma membrane marker DiI-C18 (Dong, Wang et al. 2009). Scale bar = 5 μm. (**C**) ML-SA1 (0.1-10 μM for 15 or 30 min) treatment increased the release of lysosomal enzymes into the culture medium in BMMs and RAW cells. The activity of lysosomal enzyme acid phosphatase (AP) was determined using an AP activity colorimetric assay kit. The data are presented as the percentage of the activity of the released *vs.* total (released + cell-associated) enzymes. Left panels: lysosomal AP release in WT and ML1 KO BMMs. Right panels: lysosomal AP release in RAW 264.7, ML1 O/E, and ML1 KD RAW macrophages. **(D)** Lack of an effect of ML-SA1 on the release of cytosolic enzyme LDH. **(E)** Ionomycin-induced lysosomal enzyme acid phosphatase (AP) release/activity was comparable but slightly reduced in ML1 KO BMMs. The data are presented as the percentage of the activity of the released enzymes *versus* total (released + cell-associated) enzymes. (**F**) The effects of intracellular and extracellular Ca^{2+} on ML-SA1 (10 μM for 30 min) -induced lysosomal AP release. BAPTA-AM (500 nM) and EGTA (2 mM with no added extracellular Ca^{2+}) were used to chelate intracellular and extracellular Ca^{2+}, respectively. **(G)** An increase in GCaMP3 fluorescence was observed at the uptake site of large beads (6 μm). **(H)** Selected image frames of a RAW cell doubly-transfected with GCaMP3-ML1-KK and Syt VII-mCherry. No significant GCaMP3 fluorescence increase was observed at the site of IgG-RBC uptake and cell body (whole-cell region). **(I)** Time-dependent change of the GCaMP3-ML1-KK fluorescence signal upon particle binding. For all panels, scale bars = 10 μm. For all panels, unless otherwise indicated, the data represent the mean ± the standard error of the mean (SEM) from at least three independent experiments.

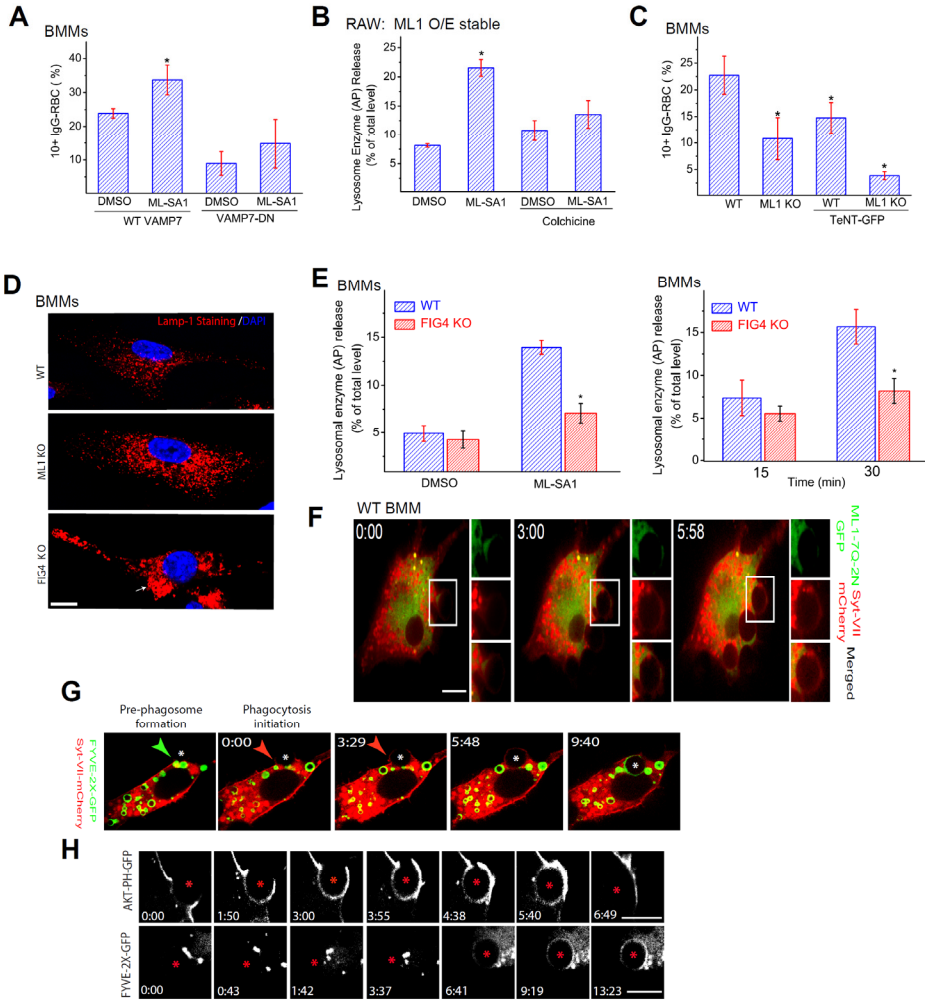

Suppl. Fig. S6. Requirement of PI(3,5)P_2 and lysosomal exocytosis in particle uptake--- Related to Figure 6.

(A) ML-SA1 (10 µM) failed to increase particle ingestion in BMMs transfected with a VAMP7 dominant-negative (VAMP7-DN) construct. **(B)** Colchicine (10 µM) inhibited ML-SA1-induced acid phosphatase (AP) release in WT BMMs. **(C)** TeNT toxin reduced particle uptake in both WT and ML1 KO BMMs. **(D)** Enlargement of Lamp1-positive compartments in FIG4 KO BMMs. Scale bar = 5 µm. **(E)** ML-SA1 (10 µM; left panel)-induced and IgG-RBC (30 min; right panel)-induced lysosomal AP release was reduced in BMMs from FIG4 KO mice. **(F)** Lack of ML1-7Q-2N-GFP accumulation at the site of uptake. Scale bar = 5 µm. **(G)** While Syt-VII-mCherry appeared on the forming phagosomes within 3-5 min of phagocytosis initiation, 2X-FYVE-GFP (PI(3)P probe) appeared on phagosomal membranes several minutes later (9 min 40 sec). The center of the particle is indicated with an *. **(H)** Distinct recruitment kinetics of AKT-PH-GFP (PI(3,4,5)P_3/PI(3,4)P_2 probe) and 2X-FYVE-GFP (PI(3)P probe) to forming phagosomes. Scale bars = 10 µm. For all panels, unless otherwise indicated, the data represent the mean ± the standard error of the mean (SEM) from at least three independent experiments.

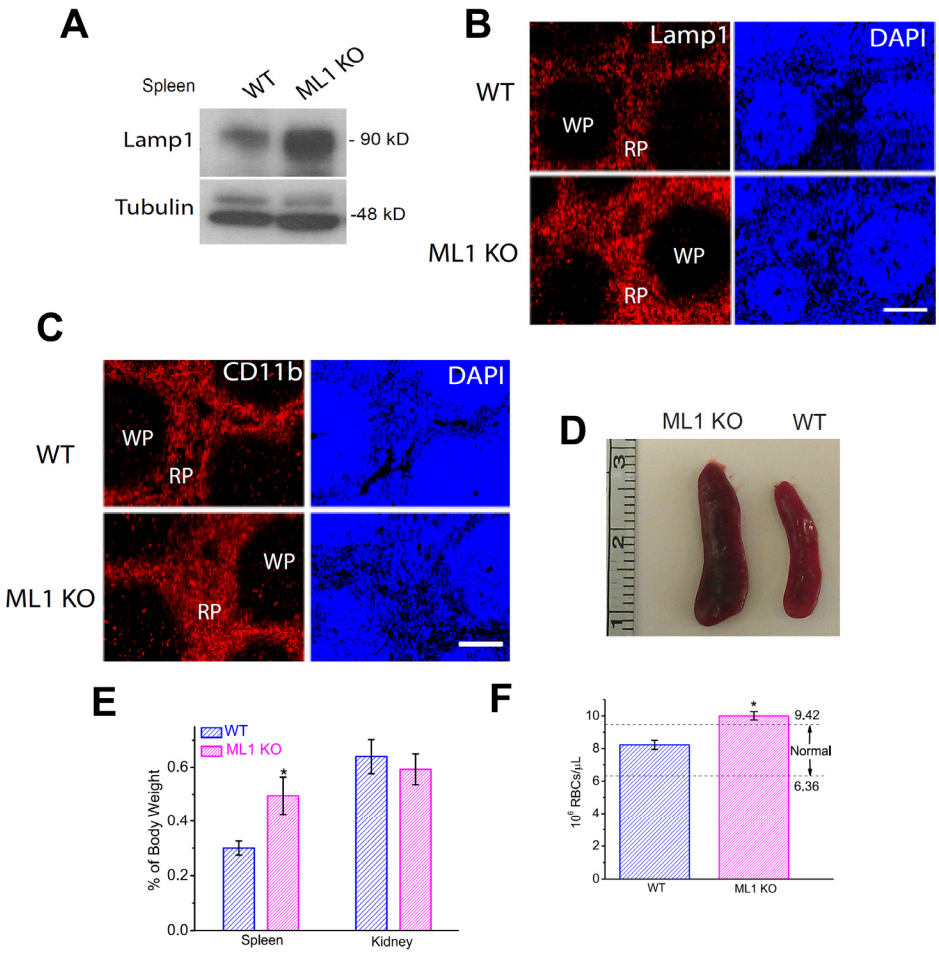

Suppl. Fig. S7. Defective clearance of senescent red blood cells in the spleen of ML1 KO mice---Related to Figure 7.

(A) An increased expression of Lamp1 proteins in ML1 KO spleens. **(B, C)** Immunofluorescence staining of Lamp1 and CD11b in the spleen sections of WT and ML1 KO mice. While Lamp1 immunefluorescence was elevated in the red pulp (RP) region of the ML1 KO spleen sections (**B**), the CD11b staining was comparable between WT and ML1 KO mice (**C**). DAPI: nucleus staining. **(D)** Representative images of spleens from 4-month-old WT and ML1 KO mice. **(E)** Normalized weight of spleens and kidneys from 4-month-old mice (N=5 animals for each). **(F)** ML1 KO mice have an elevated level of total red blood cell count compared with WT controls. Blood samples (100 µl) were collected from the mouse tails, and then placed into EDTA-containing tubes before counting (N=5 animals for each genotype). For all panels, scale bars = 200 µm. For all panels, unless otherwise indicated, the data represent the mean ± the standard error of the mean (SEM) from at least three independent experiments.

Supplemental Movie Legends

Video 1. A time-lapse video of a ML1-GFP-transfected RAW cells that were exposed to IgG-opsonized 6 μm beads (experiments conditions and snapshot images see **Fig. 3A** and figure legends).

Video 2. A time-lapse video of a ML1-GFP-transfected RAW cells that were exposed to IgG-RBCs (experiments conditions and snapshot images see ***Suppl. Fig. S3A*** and figure legends).

Video 3. Simultaneous recruitment of ML1-GFP and Syt-VII-mCherry to the IgG-RBC uptake sites (experiments conditions and snapshot images see **Fig. 3B** and figure legends).

Video 4. Transient accumulation of ML1-2N-GFP to the phagocytic cups (experiments conditions and snapshot images see **Fig. 6G** and figure legends).

Supplemental Experimental Procedures

Mouse lines. The generation and characterization of ML1 (Venugopal, Browning et al. 2007) and FIG4 KO mice (Chow, Zhang et al. 2007) have been described previously. Animals were used under approved animal protocols and Institutional Animal Care Guidelines at the University of Michigan.

Real-Time Semi-quantitative PCR. Total RNA was extracted from bone marrow-derived macrophages (BMMs) dissolved in TRIzol (Invitrogen). First strand cDNA, synthesized using Superscript III RT (Invitrogen), was used for Semi-quantitative PCR (Bio-Rad iQ iCycler) analysis of ML1 expression based on the following intron-spanning primer pair:
Forward: AAACACCCCAGTGTCTCCAG; Reverse: GAATGACACCGACCCAGACT

Macrophage cell culture. Murine BMMs were prepared and cultured as described previously (Link, Park et al. 2010). Briefly, bone marrow cells from mouse femurs and tibias were harvested and cultured in macrophage differentiation medium (RPMI-1640 medium with 10% fetal bovine serum (FBS) and 100 unit/ml recombinant colony stimulating factor (PeproTech, Rocky Hill, NJ). After 7 days in culture at 37 °C with 5% CO_2, the adherent cells (> 95% are expected to be macrophages) were harvested for assays. RAW 264.7, RAW cells stably-expressing ML1 (ML1 overexpression or O/E), and RAW cells stably-expressing ML1-specific RNAi (ML1 knockdown or KD) (Thompson, Schaheen et al. 2007) were kindly provided by Dr. Hanna Fares (University of Arizona), and cultured in DMEM/F12 media supplemented with 10% FBS at 37°C and 5% CO_2.
BMM and RAW macrophages were transfected using electroporation (Invitrogen Neon Transfection System) according to the manufacture procedures. Briefly, cells were harvested and washed with PBS (Ca^{2+} and Mg^{2+}-free) once to remove DMEM. Cells were then centrifuged and the pellets were re-suspended in the R buffer. 2 μg of DNA per well was add to the cells, which were gently mixed and placed in the Neon System pipette. The electroporation was performed using program # 6 for RAW cells and program # 18 for BMMs, respectively. Transfected cells were then recovered with 500 μl of culture media in each plate.

Whole-endolysosome electrophysiology. Endolysosomal electrophysiology was performed in isolated endolysosomes using a modified patch-clamp method as described previously (Dong, Cheng

et al. 2008; Dong, Shen et al. 2010). Briefly, cells were treated with 1 μM vacuolin-1 for 2-5h to increase the size of endosomes and lysosomes. Whole-endolysosome recordings were performed on isolated enlarged endolysosomes. The bath (internal/cytoplasmic) solution contained 140 mM K-gluconate, 4 mM NaCl, 1 mM EGTA, 2 mM Na_2-ATP, 2 mM $MgCl_2$, 0.39 mM $CaCl_2$, 0.2 mM GTP, and 10 mM HEPES (pH adjusted with KOH to 7.2; free $[Ca^{2+}]_i$ was estimated to be ~ 100 nM using the Maxchelator software (http://maxchelator.stanford.edu/)). The pipette (luminal) solution consisted of a 'Low pH Tyrode's solution' with 145 mM NaCl, 5 mM KCl, 2 mM $CaCl_2$, 1 mM $MgCl_2$, 10 m M HEPES,10 mM MES, and 10 mM glucose (pH 4.6). All bath solutions were applied via a perfusion system to achieve a complete solution exchange within a few seconds. Data were collected using an Axopatch 2A patch clamp amplifier, Digidata 1440, and pClamp 10.0 software (Axon Instruments). Currents were digitized at 10 kHz and filtered at 2 kHz. All experiments were conducted at room temperature (21-23 ºC), and all recordings were analyzed with pClamp 10.0, and Origin 8.0 (OriginLab, Northampton, MA).

Whole-cell electrophysiology. Whole-cell recordings were performed as described previously (Shen, Wang et al. 2012; Wang, Zhang et al. 2012). The pipette solution contained 147 mM Cs, 120 mM methane-sulfonate, 4 mM NaCl, 10 mM EGTA, 2 mM Na_2-ATP, 2 mM $MgCl_2$, and 20 mM HEPES (pH 7.2; free $[Ca^{2+}]_i$ < 10 nM). The standard extracellular bath solution (modified Tyrode's solution) contained 153 mM NaCl, 5 mM KCl, 2 mM $CaCl_2$, 1 mM $MgCl_2$, 20 mM HEPES, and 10 mM glucose (pH 7.4). BMMs were incubated with IgG-RBCs at 4 °C for 20 min and then were placed at 37°C and 5% CO_2 for 5~10 min before whole-cell recordings. Dynasore (100 μM) was added when the RBCs were applied to BMMs.

Fura-2 Ca^{2+} imaging. Cells were loaded with 5 μM Fura-2 AM in the culture medium at 37 °C for 60 min. Fluorescence was recorded at different excitation wavelengths using an EasyRatioPro system (PTI). Fura-2 ratios (F_{340}/F_{380}) were used to monitor changes in intracellular $[Ca^{2+}]$ upon stimulation. Ionomycin (1 μM) was added at the conclusion of all experiments to induce a maximal response for comparison.

GCaMP3 Ca^{2+} imaging. Lysosome-targeted Ca^{2+} imaging was performed in BMMs or RAW cells that were transfected with GCaMP3-ML1 or GCaMP3-ML1-KK constructs (Shen, Wang et al. 2012). The fluorescence intensity at 470 nm (F_{470}) was monitored using an EasyRatioPro system.

Flow cytometry. BMMs were trypsinized and washed with PBS before incubation with ML-SA1 (10 μM) at 37°C for 30 min. Cells were then washed, re-suspended in 1% BSA with anti-mouse Lamp1 (1D4B) antibody on ice for 45 min, and fixed in 2% PFA for 30 min, and were then incubated with Alexa-546 conjugated anti–mouse secondary antibody (Invitrogen) at room temperature for 1h. Macrophages were then re-suspended in 0.5 ml PBS, and analyzed on a FACS Flow Cytometer (MoFlo Astrios, Beckman Coulter). At least 10,000 cells per experiment were analyzed for the forward angle scatter, the right angle scatter, and the fluorescence intensity.

Lysosomal enzyme release/activity. After incubation with ML-SA1 or IgG-RBCs, the culture medium was collected for acid phosphatase (AP) activity measurement. AP activity was measured using an AP colorimetric assay kit (Sigma), which uses p-nitrophenyl phosphate (pNPP) as a phosphatase substrate which turns yellow at a wavelength of 405 nm when dephosphorylated by AP. Lactate de-hydrogenase (LDH) activity was measured using a LDH-Cytotoxicity Assay Kit (Abcam).

Fluorescence and time-lapse imaging. Live imaging of RBC uptake by BMMs was performed on a heated stage using a Spinning Disk confocal imaging system, which consists of an Olympus IX81 inverted microscope, a 100X Oil objective NA 1.49 (Olympus, UAPON100XOTIRF), a CSU-X1 scanner (Yokogawa), an iXon EM-CCD camera (Andor), and MetaMorph Advanced Imaging acquisition software v.7.7.8.0 (Molecular Devices). For Lamp1 detection, BMMs were fixed with 4% PFA and permeabilized with 0.03% Triton X-100, and then stained with 1D4B anti–mouse Lamp1 monoclonal antibody (Iowa Hybridoma Bank). The surface expression of Lamp1 was detected in non-permeabilized macrophages using the same antibody that recognizes a luminal epitope of mouse Lamp1 (Reddy, Caler et al. 2001; Dong, Wang et al. 2009). For phalloidin staining of phagosomes, BMMs were incubated for 10 min with IgG-RBCs, fixed with 4% PFA, permeabilized with 0.03% Triton X-100 for 5 min, and labeled with phalloidin- Alexa-Fluor633 (Invitrogen) for 30 min. The $PI(3,5)P_2$ probe was generated with the tandem repeats of the ML1 N-terminal segment (residues 1–68) fused with GFP tags (Li et al.). All images were taken with the 100X objective of a Leica (TCS SP5) confocal microscope.

H&E Staining. Hematoxylin and eosin (H&E) staining was performed in 5 μm slice sections prepared from paraffin-embedded spleen tissues using microtome. The tissues were fixed with 4% PFA upon heart perfusion in 10 -12 week old WT and ML1 KO mice.

HPLC measurement of phosphoinositide levels. Raw macrophage cell lines were grown in 6 well plates to 20-30% confluence. Cells were then rinsed twice with PBS and were incubated for 48 h with the inositol labeling medium, which contained inositol-free DMEM, 10 μCi/mL of myo-[2-^{3}H] inositol (GE Healthcare), 10% (vol/vol) dialyzed FBS, 20 mM Hepes, 5 μg/mL transferrin, and 5 μg/mL insulin (Zolov, Bridges et al. 2012). Afterwards, a solution (pre-warmed to 37°C) of IgG-coated 6 μM polystyrene beads was prepared in a 1:50 ratio (macrophage:beads). After RAW cells were rinsed with PBS once, 4 ml of beads were added to each well. The plates were centrifuged briefly for 1 min at 3,000 RPM and then placed at the 37°C incubator for 1, 2, 5, and 10 min. After each time point, the un-ingested beads were removed; RAW cells were treated with 500 μl of ice-cold 4.5% (vol/vol) perchloric acid for 15 min at room temperature; plates were rotated gently every 2 min to prevent cells from drying. RAW cells were scraped off, spun at 12,000 × g for 10 min at 4 °C, and then processed for HPLC measurement. The data were analyzed as described previously (Zolov, Bridges et al. 2012).

Cell death analysis in brain slice. Brain slices were stained with propidium iodide (PI; membrane impermeant dye only enters the dying cells) and analyzed with confocal microscopy. Briefly, fresh mouse brains were sectioned into 300 μm thick slices with a vibratome sectioning system. Immediately after cutting the sections, slices were washed with cold (4°C) HBSS solution, and then incubated with PI (20 μg/ml) at 37°C for 15 min, fixed in 4% paraformaldehyde for another 30 min, and then mounted on the glass slides. To avoid damage cause by tissue preparation, images were taken 100 μm underneath the slice sections.

Measurement of splenic iron content. Spleens were completely digested in 3M hydrocholoric acid/10% trichoroacetic acid at 65°C overnight. Samples were then centrifuged to precipitate any non-digested materials. The ionic composition of the supernatant was analyzed using a Thermo Scientific Finnigan Element inductively coupled with a plasma-high resolution mass spectrometer (ICP-HRMS) (Wang, Zhang et al. 2012).

References

Chow, C. Y., Y. Zhang, et al. (2007). "Mutation of FIG4 causes neurodegeneration in the pale tremor mouse and patients with CMT4J." Nature **448**(7149): 68-72.

Dong, X. P., X. Cheng, et al. (2008). "The type IV mucolipidosis-associated protein TRPML1 is an endolysosomal iron release channel." Nature **455**(7215): 992-996.

Dong, X. P., D. Shen, et al. (2010). "PI(3,5)P(2) Controls Membrane Traffic by Direct Activation of Mucolipin Ca Release Channels in the Endolysosome." Nat Commun **1**(4).

Dong, X. P., X. Wang, et al. (2009). "Activating mutations of the TRPML1 channel revealed by proline-scanning mutagenesis." J Biol Chem **284**(46): 32040-32052.

Link, T. M., U. Park, et al. (2010). "TRPV2 has a pivotal role in macrophage particle binding and phagocytosis." Nat Immunol **11**(3): 232-239.

Reddy, A., E. V. Caler, et al. (2001). "Plasma membrane repair is mediated by Ca(2+)-regulated exocytosis of lysosomes." Cell **106**(2): 157-169.

Shen, D., X. Wang, et al. (2012). "Lipid storage disorders block lysosomal trafficking by inhibiting a TRP channel and lysosomal calcium release." Nat Commun **3**: 731.

Thompson, E. G., L. Schaheen, et al. (2007). "Lysosomal trafficking functions of mucolipin-1 in murine macrophages." BMC Cell Biol **8**: 54.

Venugopal, B., M. F. Browning, et al. (2007). "Neurologic, gastric, and opthalmologic pathologies in a murine model of mucolipidosis type IV." Am J Hum Genet **81**(5): 1070-1083.

Wang, X., X. Zhang, et al. (2012). "TPC Proteins Are Phosphoinositide- Activated Sodium-Selective Ion Channels in Endosomes and Lysosomes." Cell **151**(2): 372-383.

Zolov, S. N., D. Bridges, et al. (2012). "In vivo, Pikfyve generates PI(3,5)P2, which serves as both a signaling lipid and the major precursor for PI5P." Proc Natl Acad Sci U S A **109**(43): 17472-17477.